Available online at www.sciencedirect.com

ScienceDirect

journal homepage: www.elsevier.com/locate/he

Short Communication

Hydrogen-induced nanohardness variations in a CoCrFeMnNi high-entropy alloy

Yakai Zhao [a], *Dong-Hyun Lee* [a], *Jung-A Lee* [a], *Woo-Jin Kim* [a], *Heung Nam Han* [b], *Upadrasta Ramamurty* [c], *Jin-Yoo Suh* [d,**], *Jae-il Jang* [a,*]

[a] *Division of Materials Science and Engineering, Hanyang University, Seoul 04763, Republic of Korea*
[b] *Department of Materials Science and Engineering, Seoul National University, Seoul 08826, Republic of Korea*
[c] *Department of Materials Engineering, Indian Institute of Science, Bangalore 560012, India*
[d] *High Temperature Energy Materials Research Center, Korea Institute of Science and Technology, Seoul 02792, Republic of Korea*

ARTICLE INFO

Article history:
Received 2 January 2017
Received in revised form
8 February 2017
Accepted 9 February 2017
Available online 17 March 2017

Keywords:
High-entropy alloy
Hydrogen
Nanoindentation
Thermal desorption spectroscopy

ABSTRACT

The influence of electrochemically charged hydrogen (H) on the hardness (H_N) of a CoCrFeMnNi high-entropy alloy (HEA) was investigated with nanoindentation. Upon charging, H_N of HEA increases by ~60%, which decreases gradually during subsequent aging at room temperature, and on prolonged aging, the alloy softens to an extent that H_N falls below that of the uncharged HEA. These H-induced mechanical property variations are rationalized in terms of the competition between solid solution hardening caused by H and excess vacancy creation due to deeply trapped H.

Introduction

High entropy alloys (HEAs) reportedly possess extraordinary properties such as high strength, large strain hardening capability, high toughness (especially, at cryogenic temperatures), excellent resistance to high-temperature softening/creep, and good tribological properties [1–4]. Hence, these alloys offer promise for applications in transportation, nuclear construction, and aerospace industries [3]. Consequently, a great deal of current research interest is on these alloys. One of the crucial, but unsolved issues for the aforementioned applications is the effect of hydrogen (H) on HEA's mechanical behavior. While it is well known that exposure to H can significantly degrade the mechanical performance of most metals and alloys [5–8], such possibility was not investigated in the context of HEAs, which are likely to be exposed to H-rich environments in a number of potential application scenarios (e.g., environments of nuclear power plant water reactors [9], aircrafts [10], and vessels for H transportation/storage or

* *Corresponding author.*
** *Corresponding author.*
E-mail addresses: jinyoo@kist.re.kr (J.-Y. Suh), jijang@hanyang.ac.kr (J.-i. Jang).
http://dx.doi.org/10.1016/j.ijhydene.2017.02.061

space shuttles [11,12]). Note that the suitability of HEAs for storing H was investigated already [13–15], wherein the ability of HEAs to absorb was reported to be less than 2 wt.%. Consequently, the objective of this study is to examine the effect of H on the plastic flow resistance of a HEA (equiatomic CoCrFeMnNi) due to electrochemical charging and subsequent degassing during aging with the aid of nanoindentation experiments.

The equiatomic CoCrFeMnNi HEA examined in this study forms a stable face-centered cubic (fcc) single phase and is the most researched HEA thus far [16,17]. A wide variety of fundamental studies were performed on it and some interesting features such as increase in both strength and ductility with decreasing temperature [18,19], relatively weak strain-rate dependence [18], excellent fracture toughness (especially at cryogenic temperatures) [20], and strong grain size dependences of strength [19,21], hardness [22,23], and creep [24], were reported.

Experimental

The $Co_{20}Cr_{20}Fe_{20}Mn_{20}Ni_{20}$ (nominal composition, in at.%) HEA was prepared by vacuum induction casting of a mixture of pure metals (purity > 99 wt.%). The cast ingot was hot-forged, followed by solution-annealing for 1 h at 1100 °C to obtain fully recrystallized microstructure. Electron beam scattered diffraction (EBSD) and X-ray diffraction (XRD) analyses (see Fig. S1 of Supplementary Material) reveal that the annealed sample has a homogeneous equiaxed microstructure consisting of a single fcc phase with a lattice parameter of 3.594 ± 0.003 Å (that falls within the range of literature values, 3.59–3.61 Å, for the same composition HEA [22,25,26]) and with an average grain size of ~34 μm.

For H charging and subsequent nanoindentation, specimen surfaces were polished initially with fine SiC papers (grit number up to 2000), and then with 0.05 μm colloidal silica to a mirror finish. The final thickness of the specimens was ~300 μm. H was electrochemically introduced into the sample by cathodic charging at room temperature (RT) in 1 N H_2SO_4 solution for different times, t_c, up to 24 h under a constant current density of 100 mA/cm^2. Immediately after charging, the microstructure was examined by scanning electron microscopy (SEM) using Nova NanoSEM 450 (FEI Inc., Hillsboro, OR, USA). The hydrogenated specimens were naturally aged at RT for different time spans, t_a, to evaluate the effect of H desorption on properties. Hereafter, the samples charged for X h will be referred to as “XC” while the sample aged for Y h will be described as “YA.” Thus, for example, a sample charged for 24 h and then aged for 24 h will be referred to as “24C + 24A.”

In selected samples, the amount of absorbed H is quantified by recourse to thermal desorption spectroscopy (TDS) equipped with a quadrupole mass spectroscope (EX0014, R-DEC Company, Tsukuba, Japan). During TDS, hydrogenated samples were heated at a constant rate of 5 °C/min, and the flow of the desorbed H_2 gas was recorded with an accuracy of 0.01 weight ppm (wppm). For TDS, the charged samples were immediately immersed into liquid nitrogen and kept until the measurement.

Nanoindentation experiments were conducted using a Nanoindenter-XP (formerly MTS; now Keysight Technologies, Oak Ridge, TN, USA) with two three-sided pyramidal indenters (typical Berkovich and sharper cube-corner tips) with a peak load, P_{max}, of 100 mN under constant indentation strain rate [27], $\dot{\varepsilon} = (dh/dt)/h = 0.025\ s^{-1}$. To minimize the influence of H outgassing, each test was always finished within 2 h after charging or natural aging. At least 10–15 indentations were conducted for each condition. After nanoindentation, hardness impressions were profiled with an atomic force microscope (AFM; XE-100, Park Systems, Suwon, Korea).

Results and discussion

Representative load–displacement (P–h) curves of uncharged (UC), charged, and charged-then-aged specimens are provided in Fig. 1a. The maximum displacement at the peak load, h_{max}, decreases with increasing charging time, t_c, and increases with aging time, t_a. From the plots, the nanoindentation hardness, H_N, values were estimated by using the Oliver–Pharr method [28]. Variation in H_N as a function of t_a and t_c is displayed in Fig. 1b. A marked increase in H_N with t_c can be noted, from ~2.7 (UC) to a maximum ~4.4 GPa (24C). Similar to the case of conventional metals and alloys, this H-induced hardening in HEA can be attributed to solid solution strengthening that enhances the resistance to dislocation motion [29,30] and H-enhanced slip planarity [31,32]. A marked reduction in H_N upon aging of the hydrogenated sample, with H_N decreasing to that of the UC sample, after $t_a \approx 24$ h is noteworthy. The fact that it takes only ~24 h for H_N to reduce back to that of UC condition of the HEA is striking, especially since such recovery is usually reported to take much longer time (ranging from a week to a month) in the case of conventional fcc metals and alloys [33,34]. Aging beyond 24 h leads to a further reduction in H_N, leading to a H_N that is even lower than the H_N of the UC alloy.

Next, the pile-ups around the nanoindentations were examined. Cube-corner indenter was utilized for this purpose, as it produces significantly higher stresses and strains underneath the indenter and thus more pronounced pile-up (if any) than the Berkovich indenter [35]. The obtained surface profiles of hardness impression are shown in Fig. 2 where representative AFM images are also provided. Two interesting features are noteworthy. First, the pile-up is less pronounced in the hydrogenated specimen (24C), which may be due to the reduced propensity for cross slip—and hence plasticity—underneath the indenter because of the H present in the alloy [31,32]. Second, and more interestingly, the pile-up height further decreases due to aging (24C + 24A) rather than getting restored back to that of the initial (UC) state. Combining this observation with the fact that the long-term aged samples (e.g., 24C + 48A sample in Fig. 1) exhibit even lower H_N than that of UC sample, it is reasonable to conclude that the observed softening after long-term aging may not be an artifact and also not be purely due to H outgassing. Instead, these observations point to some irreversible microstructural change(s) induced by H. It is important to note here that although pile-up is known to cause overestimation of H_N

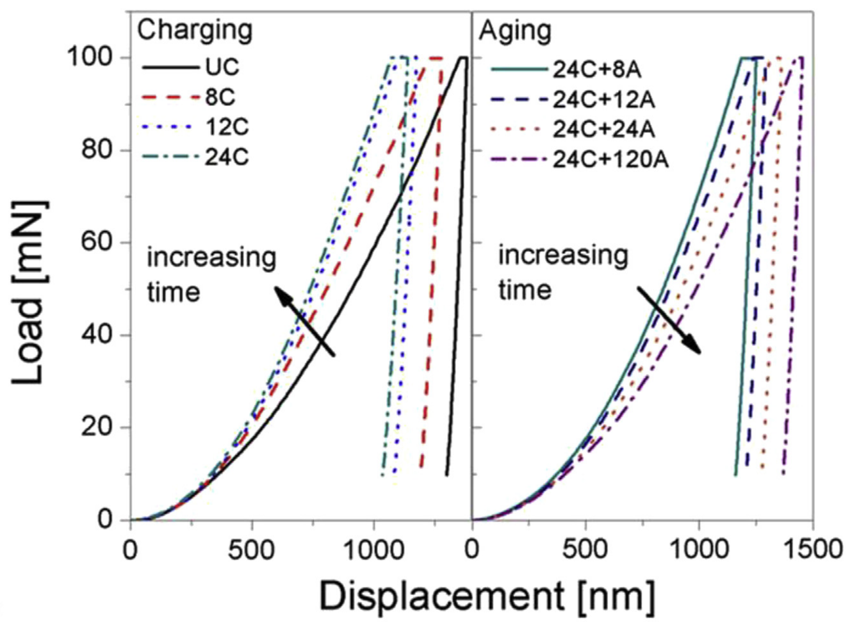

(a)

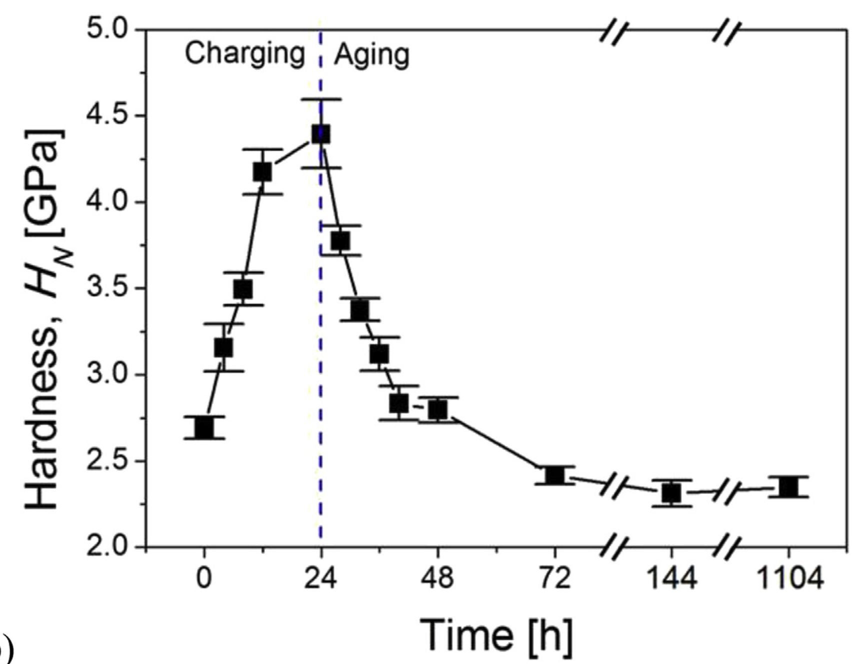

(b)

Fig. 1 – Results of nanoindentation; (a) representative *P*–*h* curves of uncharged, charged, and charged-then-aged specimens; (b) variation in nanoindentation hardness, H_N, as a function of the time for charging and aging.

obtained by Oliver–Pharr method, the direct measurements of the indentation impression areas by using SEM [36] were conducted on UC, 24C, 24C + 24A and 24C + 120A samples and the results are shown in Table 1, confirming that the trend of H_N change in Fig. 1b is for real.

To gain insight into the mechanisms responsible for the observed fast H diffusivity and the possible H-induced microstructural changes, TDS analysis was performed on UC, 24C, 24C + 24A, and 24C + 120A samples, and the resultant desorption plots are displayed in Fig. 3. It is seen that the 24C specimen indeed contains a large amount of H (~45 wppm), which reduces rapidly to ~14.2 wppm in upon aging for 24 h (24C + 24A sample). Aging for 120 h leads to further reduction in H, to ~7.2 wppm in 24C + 120A specimen. Note that this quantity of H is about four times higher than that in UC sample (~1.7 wppm). This rationalizes the observation of smaller pile-up around indents made on the 24C + 24A sample vis-á-vis that of the UC sample (see Fig. 2). It further leads us to conclude that even after long-term aging, the condition of the once-charged sample is different from that of UC sample, i.e., absorption and desorption of H induce irreversible changes in HEA. In consideration of (1) the strong ability of

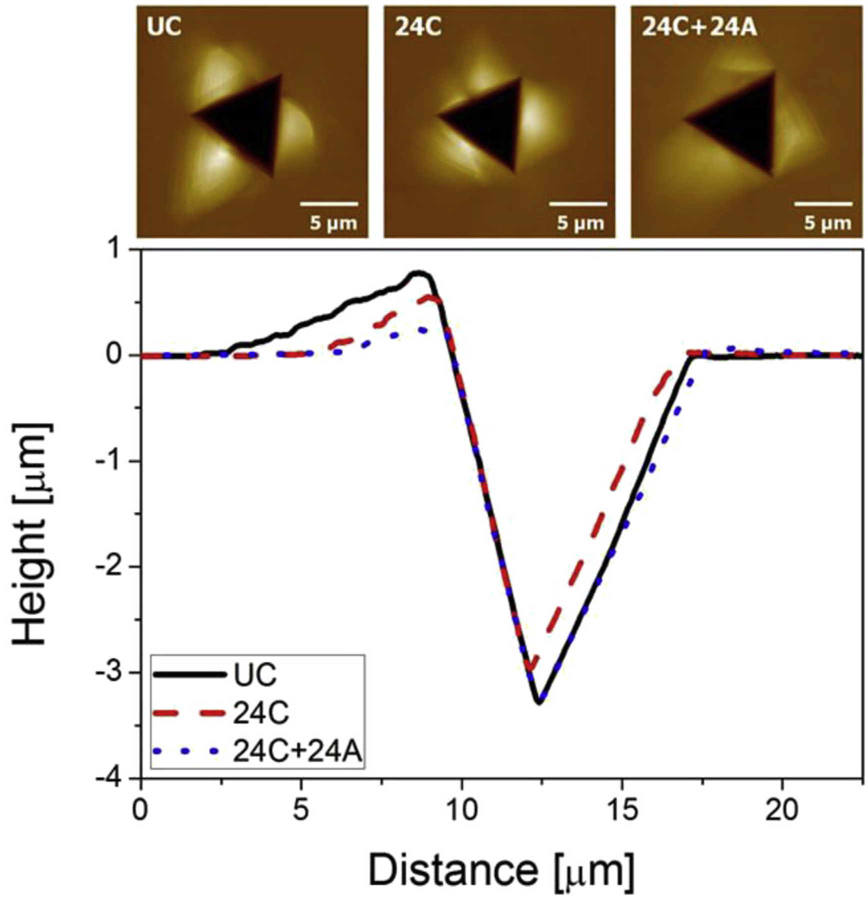

Fig. 2 – Surface height profiles of cube-corner indentations (with representative AFM images on the top).

electrochemical charging method to introduce H into a given alloy [37,38] and (2) relatively low diffusivity of H in metals with fcc crystal structure [39], it is reasonable to expect that H atoms in this CoCrFeMnNi alloy are highly concentrated near surface [38]. By adopting the method used by Pontini and Hermida [40], the local H concentration near the surface of an electro-chemically charged specimen, C_0, can be estimated in an approximate manner as

$$C_0 = \frac{w \cdot C_M}{4}\sqrt{\frac{\pi}{D_H t_c}} \tag{1}$$

where w is sample thickness (300 μm here), C_M is the mean H concentration of the sample (~45 wppm for 24C sample), and D_H is H diffusivity. We further assume that D_H for CoCrFeMnNi HEA is similar to that of austenitic stainless steel (ASS), since (1) both have fcc structure, (2) the chemical constituents are identical [4], and (3) D_H of ASS is reported to be nearly-insensitive to the composition [41]. Taking D_H of ASS (~3.17×10^{-16} m^2/s at RT [41]) into Eq. (1), C_0 was estimated to be ~1143 wppm. Such a large value for C_0 indicates that H indeed is highly concentrated near the surface (within ~60 μm from the surface based on the calculation in Ref. [40]) and its local H concentration can theoretically reach as high as in the order of ~10^3 wppm. Since nanoindentation technique probes the near-surface properties of the material, it is natural that such high H concentration near surface affects the measured

Table 1 – Nanoindentation hardness values of representative specimens obtained by both Oliver–Pharr method and direct estimations from SEM images.

	Nanoindentation hardness [GPa]			
	UC	24C	24C + 24A	24C + 120A
Oliver–Pharr	2.69 ± 0.06	4.39 ± 0.20	2.80 ± 0.07	2.31 ± 0.08
SEM	2.24 ± 0.07	2.71 ± 0.19	2.43 ± 0.10	2.03 ± 0.09

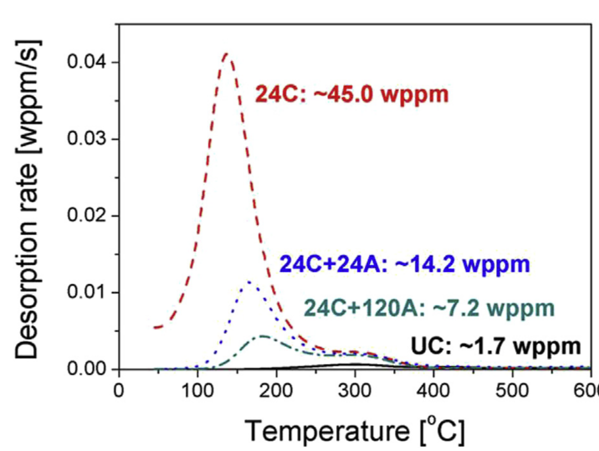

Fig. 3 – TDS curves of representative samples.

properties in a marked manner. The high C_0 at surface has two consequences. First is through solid solution strengthening effect of H, which results in the marked increase in H_N with charging time (and thus with H content) [42]. Second, it will provide a strong driving force for H to desorb out of the specimen surface, which is evidenced by the significantly high desorption rate in 24C sample even at the early stage of heating in TDS test (~0.005 wppm/s) as shown in Fig. 3, leading to the fast H outgassing and thus the quick H_N recovery upon aging.

In addition to H content, the TDS plots in Fig. 3 also provide information about the interactions between H and microstructures since a distinction between different H traps can be drawn based on the two different peaks for H desorption (at ~150 and ~300 °C, respectively). A higher-temperature peak corresponds to stronger H-trapping sites which have higher H-binding energies and require a higher temperature to release the trapped H [7,38]. Since no new metallic hydride phase was found in the HEA after H charging (as evidenced by XRD measurements shown in Fig. S2 of the Supplementary Material), it is expected from previous studies on fcc metals and alloys that the peak at low temperature corresponds to interstitial lattice sites and weak H trapping defects such as dislocations whereas the high-temperature peak may be attributed to relatively strong H trapping sites such as vacancies [43,44]. From the observation that the intensity of the high-temperature peak remains unaltered during aging, vacancies can be categorized as irreversible H trapping sites. Note that the H trapping energy of dislocations is usually slightly lower in fcc than the activation energy for the bulk diffusion of H and thus desorption peaks of such weak trapping sites tend to overlap with that of fcc lattice [45,46].

In crystalline metals and alloys, the attraction between interstitial H and vacancies is known to induce a higher equilibrium concentration of vacancies in H-containing metals than in uncharged metals, which is often referred to as "superabundant vacancy" formation [47,48]. Such H-induced excess vacancies can lead to the growth of voids and bubbles, then increase local plasticity, and eventually promote fracture process [49]. Another concomitant effect of the increased vacancy concentration is lattice contraction (manifested as the decrease in lattice parameter [43]) which can result in intergranular cracking due to resultant tensile stresses at grain boundaries (GBs) exceeding the GB strength [50]. In the present study, indeed, cracks were often found along GBs on the surfaces of the hydrogenated specimens, as seen in Fig. 4, which may be construed as an indirect evidence for the H-induced enhancement of vacancy concentrations in the specimens. We note here that the nanoindentations were always made in the crack-free areas to avoid the effects of the cracks on the measured H_N.

Finally, possible reasons for the slight softening in the long-term-aged specimens are the following. From Fig. 3 we see that only the intensity of the low-temperature peak continuously decreases upon aging, whereas the intensity of the high-temperature peak remains unaltered. Since the high-temperature peak corresponds to the trapping sites of vacancies, the nearly constant intensity of this peak indicates that although the H located in interstitial and weak trapping defects quickly desorbs out of the specimen during aging, the

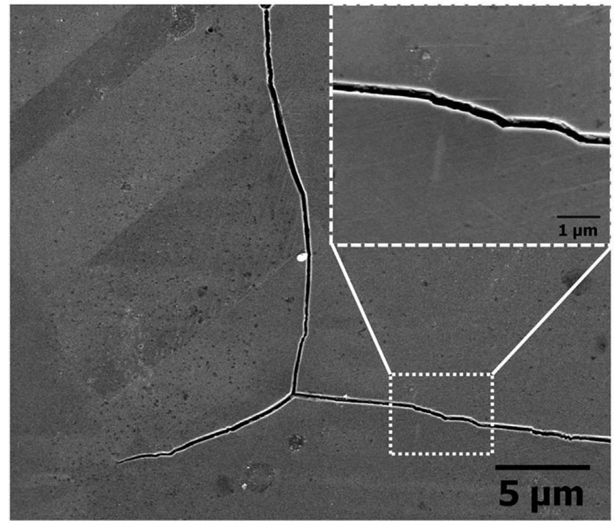

Fig. 4 – Typical SEM image showing surface cracks along grain boundaries in 24C specimen (with enlarged image in inset).

H trapped in vacancies is rather stable (due to a relatively high H binding energy of vacancies [51]) and does not desorb at RT. Thus, upon aging at RT, vacancies would still exist in the specimens due to the stabilization by the trapped H atoms and are not annihilated, which is also indirectly evidenced by intergranular cracking, as already mentioned. Since high vacancy concentration can lead to a non-negligible softening [44], a competition between hardening (by solid solution strengthening of H) and softening (by vacancies) may occur. With continued aging, the solid solution strengthening of H continuously decreases due to H outgassing, while the contribution of the vacancies to softening remains invariant. Eventually, after over 24 h aging, most of H desorbs out of the specimen and the softening effect of vacancies becomes predominant.

Conclusion

In summary, the influences of electrochemical H charging and subsequent aging on the hardness of CoCrFeMnNi HEA were investigated. The results reveal that upon charging, the alloy's hardness increases significantly, which is due to solid solution strengthening caused by H especially near the surface. Subsequent aging at room temperature leads to reduction in hardness, due to degassing. Prolonged aging results in an alloy whose hardness is even slightly lower than that of uncharged specimen. This softening is attributed, with the aid of TDS and microstructural observations, to superabundant vacancy formation caused by H.

Acknowledgments

The work at Hanyang University was supported by the National Research Foundation of Korea (NRF) grants funded by the Ministry of Science, ICT & Future Planning (MSIP) (No. 2014M2A8A1030385 and No. 2015R1A5A1037627). The work at KIST was supported by the Convergence Agenda Program (CAP) of the Korea Research Council of Fundamental Science and Technology. The authors wish to thank Mr. Han-Jin Kim (KIST) for the valuable supports for the experimental work.

Appendix A. Supplementary data

Supplementary data related to this article can be found at http://dx.doi.org/10.1016/j.ijhydene.2017.02.061.

REFERENCES

[1] Zhang Y, Zuo TT, Tang Z, Gao MC, Dahmen KA, Liaw PK, et al. Microstructures and properties of high-entropy alloys. Prog Mater Sci 2014;61:1–93.
[2] Gao MC, Yeh J-W, Liaw PK, Zhang Y, editors. High-entropy alloys: fundamentals and applications. Switzerland: Springer; 2016.
[3] Ye YF, Wang Q, Lu J, Liu CT, Yang Y. High-entropy alloy: challenges and prospects. Mater Today 2016;19:349–62.
[4] Miracle DB, Senkov ON. A critical review of high entropy alloys and related concepts. Acta Mater 2017;122:448–511.
[5] Hirth JP. Effects of hydrogen on the properties of iron and steel. Metall Trans A 1980;11:861–90.
[6] Lee J-A, Lee D-H, Seok M-Y, Baek UB, Lee Y-H, Nahm SH, et al. Hydrogen-induced toughness drop in weld coarse-grained heat-affected zones of linepipe steel. Mater Charact 2013;82:17–22.
[7] Zhao Y, Choi I-C, Seok M-Y, Kim M-H, Kim D-H, Ramamurty U, et al. Effect of hydrogen on the yielding behavior and shear transformation zone volume in metallic glass ribbons. Acta Mater 2014;78:213–21.
[8] Gangloff RP, Somerday BP, editors. Gaseous hydrogen embrittlement of materials in energy Technologies. Cambridge: Woodhead Publishing Ltd; 2012.
[9] Dutta RS. Corrosion aspects of Ni–Cr–Fe based and Ni–Cu based steam generator tube materials. J Nucl Mater 2009;393:343–9.
[10] Hénaff G, Odemer G, Tonneau-Morel A. Environmentally-assisted fatigue crack growth mechanisms in advanced materials for aerospace applications. Int J Fatigue 2007;29:1927–40.
[11] Barthélémy H. Hydrogen storage – industrial prospective. Int J Hydrogen Energy 2012;37:17364–72.
[12] Boyer RR. An overview on the use of titanium in the aerospace industry. Mater Sci Eng A 1996;213:103–14.
[13] Kao Y-F, Chen S-K, Sheu J-H, Lin J-T, Lin W-E, Yeh J-W, et al. Hydrogen storage properties of multi-principal-component $CoFeMnTi_xV_yZr_z$ alloys. Int J Hydrogen Energy 2010;35:9046–59.
[14] Kunce I, Planski M, Bystrzycki J. Structure and hydrogen storage properties of a high entropy ZrTiVCrFeNi alloy synthesized using Laser Engineered Net Shaping (LENS). Int J Hydrogen Energy 2013;38:12180–9.
[15] Kunce I, Planski M, Bystrzycki J. Microstructure and hydrogen storage properties of a TiZrNbMoV high entropy alloy synthesized using Laser Engineered Net Shaping (LENS). Int J Hydrogen Energy 2014;39:9904–10.
[16] Cantor B, Chang ITH, Knight P, Vincent A. Microstructural development in equiatomic multicomponent alloys. Mater Sci Eng A 2004;375–377:213–8.
[17] Otto F, Hanold NL, George EP. Microstructural evolution after thermomechanical processing in an equiatomic, single-phase CoCrFeMnNi high-entropy alloy with special focus on twin boundaries. Intermetallics 2014;54:39–48.
[18] Gali A, George EP. Tensile properties of high- and medium-entropy alloys. Intermetallics 2013;39:74–8.
[19] Otto F, Dlouhý A, Somsen Ch, Bei H, Eggeler G, George EP. The influences of temperature and microstructure on the tensile properties of a CoCrFeMnNi high-entropy alloy. Acta Mater 2013;61:5743–55.
[20] Gludovatz B, Hohenwarter A, Catoor D, Chang EH, George EP, Ritchie RO. A fracture-resistant high-entropy alloy for cryogenic applications. Science 2014;345:1153–8.
[21] Schuh B, Mendez-Martin F, Völker B, George EP, Clemens H, Pippan R, et al. Mechanical properties, microstructure and thermal stability of a nanocrystalline CoCrFeMnNi high-entropy alloy after severe plastic deformation. Acta Mater 2015;96:258–68.
[22] Liu WH, Wu Y, He JY, Nieh TG, Lu ZP. Grain growth and the Hall–Petch relationship in a high-entropy FeCrNiCoMn alloy. Scr Mater 2013;68:526–9.
[23] Lee D-H, Choi I-C, Seok M-Y, He J, Lu Z, Suh J-Y, et al. Nanomechanical behavior and structural stability of a nanocrystalline CoCrFeNiMn high-entropy alloy processed by high-pressure torsion. J Mater Res 2015;30:2804–15.
[24] Lee D-H, Seok M-Y, Zhao Y, Choi I-C, He J, Lu Z, et al. Spherical nanoindentation creep behavior of nanocrystalline and coarse-grained CoCrFeMnNi high-entropy alloys. Acta Mater 2016;109:314–22.
[25] Zhu C, Lu ZP, Nieh TG. Incipient plasticity and dislocation nucleation of FeCoCrNiMn high-entropy alloy. Acta Mater 2013;61:2993–3001.
[26] Stepanov ND, Shaysultanov DG, Salishchev GA, Tikhonovsky MA, Oleynik EE, Tortika AS, et al. Effect of V content on microstructure and mechanical properties of the $CoCrFeMnNiV_x$ high entropy alloys. J Alloys Compd 2015;628:170–85.
[27] Lucas BN, Oliver WC. Indentation power-law creep of high-purity indium. Metall Mater Trans A 1999;30:601–10.
[28] Oliver WC, Pharr GM. An improved technique for determining hardness and elastic modulus using load and displacement sensing indentation experiments. J Mater Res 1992;7:1564–83.
[29] Barnoush A, Asgari M, Johnsen R. Resolving the hydrogen effect on dislocation nucleation and mobility by electrochemical nanoindentation. Scr Mater 2012;66:414–7.
[30] Asgari M, Johnsen R, Barnoush A. Nanomechanical characterization of the hydrogen effect on pulsed plasma nitrided super duplex stainless steel. Int J Hydrogen Energy 2013;38:15520–31.
[31] Morasch KR, Bahr DF. The effects of hydrogen on deformation and cross slip in a BCC titanium alloy. Scr Mater 2001;45:839–45.
[32] Nibur KA, Bahr DF, Somerday BP. Hydrogen effects on dislocation activity in austenitic stainless steel. Acta Mater 2006;54:2677–84.
[33] Ieki Y, Asano S. Hydrogen-induced hardening and embrittlement in FCC Fe-Ni-Mn alloys subjected to cathodic charging. J Jpn Inst Met 1994;58:1008–14.
[34] Panagopoulos CN, Zacharopoulos N. Cathodic hydrogen charging and mechanical properties of copper. J Mater Sci 1994;29:3843–6.
[35] Jang J-I, Pharr GM. Influence of indenter angle on cracking in Si and Ge during nanoindentation. Acta Mater 2008;56:4458–69.
[36] Zhao Y, Choi I-C, Seok M-Y, Ramamurty U, Suh J-Y, Jang J-I. Hydrogen-induced hardening and softening of Ni–Nb–Zr

amorphous alloys: dependence on the Zr content. Scr Mater 2014;93:56–9.

[37] Brass A-M, Chêne J. Hydrogen uptake in 316L stainless steel: consequences on the tensile properties. Corros Sci 2006;48:3222–42.

[38] Zhao Y, Seok M-Y, Choi I-C, Lee Y-H, Park S-J, Ramamurty U, et al. The role of hydrogen in hardening/softening steel: influence of the charging process. Scr Mater 2015;107:46–9.

[39] Turnbull A. Hydrogen diffusion and trapping in metals. In: Gangloff RP, Somerday BP, editors. Gaseous hydrogen embrittlement of materials in energy technologies. Cambridge: Woodhead Publishing Ltd; 2012. p. 89–128.

[40] Pontini AE, Hermida JD. X-ray diffraction measurement of the stacking fault energy reduction induced by hydrogen in an AISI 304 steel. Scr Mater 1997;37:1831–7.

[41] San Marchi C, Somerday BP, Robinson SL. Permeability, solubility and diffusivity of hydrogen isotopes in stainless steels at high gas pressures. Int J Hydrogen Energy 2007;32:100–16.

[42] Yao Y, Pang X, Gao K. Investigation on hydrogen induced cracking behaviors of Ni-base alloy. Int J Hydrogen Energy 2011;36:5729–38.

[43] Fukai Y, Mizutani M, Yokota S, Kanazawa M, Miura Y, Watanabe T. Formation of superabundant vacancies in M–H alloys and some of its consequences: a review. J Alloys Compd 2003;356–357:270–3.

[44] Zhao Y, Seok M-Y, Lee D-H, Lee J-A, Suh J-Y, Jang J-I. Hydrogen-induced softening in nanocrystalline Ni investigated by nanoindentation. Philos Mag 2016;96:3442–50.

[45] Ryu JH, Chun YS, Lee CS, Bhadeshia HKDH, Suh DW. Effect of deformation on hydrogen trapping and effusion in TRIP-assisted steel. Acta Mater 2012;60:4085–92.

[46] Lee S-M, Lee J-Y. The trapping and transport phenomena of hydrogen in nickel. Metall Trans A 1986;17:181–7.

[47] Fukai Y. The metal-hydrogen system. Berlin: Springer; 2005.

[48] Carr NZ, McLellan RB. The thermodynamic and kinetic behavior of metal–vacancy–hydrogen systems. Acta Mater 2004;52:3273–93.

[49] Nagumo M, Nakamura N, Takai K. Hydrogen thermal desorption relevant to Delayed-fracture susceptibility of high-strength steels. Metall Mater Trans A 2001;32:339–47.

[50] Kim YS, Maeng WY, Kim SS. Effect of short-range ordering on stress corrosion cracking susceptibility of Alloy 600 studied by electron and neutron diffraction. Acta Mater 2015;83:507–15.

[51] Kuhn DK, Johnson HH. Transient analysis of hydrogen permeation through nickel membranes. Acta Metall Mater 1991;39:2901–8.